Reflectivity in shock wave fronts of xenon

2006 J. Phys. A: Math. Gen. 39 4393

(http://iopscience.iop.org/0305-4470/39/17/S13)

INSTITUTE OF PHYSICS PUBLISHING JOURNAL OF PHYSICS A: MATHEMATICAL AND GENERAL

J. Phys. A: Math. Gen. **39** (2006) 4393–4399 doi:10.1088/0305-4470/39/17/S13

Reflectivity in shock wave fronts of xenon

T Raitza[1], H Reinholz[1], G Röpke[1], V Mintsev[2] and A Wierling[1]

[1] Institute of Physics, University of Rostock, 18051 Rostock, Germany
[2] Institute of Problems of Chemical Physics, Chernogolovka, Russia

E-mail: heidi.reinholz@uni-rostock.de

Received 6 October 2005, in final form 15 December 2005
Published 7 April 2006
Online at stacks.iop.org/JPhysA/39/4393

Abstract

New results for the reflection coefficient of shock-compressed dense xenon plasmas at pressures of 1.6–20 GPa and temperatures around 30 000 K are interpreted. Reflectivities typical of metallic systems are found at high densities. A consistent description of the measured reflectivities is achieved if a finite width of the shock wave front is considered. Several mechanisms to give a microscopic explanation for a finite extension of the shock front are discussed.

PACS numbers: 52.25.Fi, 52.25.Mq, 52.27.Gr, 52.38.Dx

1. Introduction

The measurement of the optical reflectivity on dense plasmas is an important diagnostic tool. In particular, it is expected that information about thermodynamic parameters, such as the density n_e of free charge carriers, can be deduced. Reflectivity measurements in dense xenon plasmas, which were produced by intense shock waves, have been performed with a laser beam of wavelength 1.06 μm [1]. Recently, measurements at a second wavelength of 0.694 μm [2, 3] using the same experimental set-up have become available. Data at a third wavelength of 0.532 μm are reported in this volume [4]. For laser frequencies $\omega_L = 2\pi c/\lambda$ above the plasma frequency $\omega_{pl} = (n_e e^2/\epsilon_0 m_e)^{1/2}$, it is expected that the plasma becomes transparent. For the frequencies used here this relates to critical densities $n_e^{cr} = \epsilon_0 m_e \omega_L^2/e^2$, as shown in table 1.

However, at temperatures around 30 000 K, an increase of the reflectivity indicating the onset of metallic behaviour was observed for densities only above the critical density.

The reflectivity on step-like plasma fronts can be calculated via the Fresnel formula [5]. Then, the reflectivity is directly related to the dielectric function which is calculated via a generalized Drude formula [6, 7]

$$\epsilon(\omega) = 1 - \frac{\omega_{pl}^2}{\omega[\omega + i\nu(\omega)]}, \tag{1}$$

Table 1. Laser wavelength λ, corresponding frequency ω_L and critical density n_e^{cr}.

λ (nm)	ω_L (10^{15} Hz)	n_e^{cr} (10^{21} cm^{-3})
1060	1.78	1.0
694	2.71	2.3
532	3.53	3.9

where the dynamical collision frequency $\nu(\omega)$ is introduced. The calculation of the reflectivity is thus traced back to the evaluation of the dynamical collision frequency. This approach has been extensively investigated including strong collisions, dynamical effects and additional scattering mechanisms due to partial ionization, for details see [3, 6, 8]. But it fails to describe the experimental data on the reflectivity of xenon satisfactorily. A similar conclusion has been found by Kurilenkov *et al* [9, 10] who used a generalized Drude formula similar to equation (1), and calculated the collision frequency in slightly different approximations. Desjarlais [11] applied molecular dynamics calculations with density functional theory combined with ionization degrees taken from Gryaznov *et al* [6]. However, significant differences with the experimental data have remained. In conclusion, the steep increase of the reflectivity only at densities above the critical one cannot be explained assuming a step-like plasma front despite a highly sophisticated approach for the calculation of the dielectric function.

An explanation for the experimental data is found if the constraint of a step-like plasma front is removed. In the following, more general assumptions about the charge density profile across the shock wave front have been considered. In particular, based on measurements of the reflectivity at the third wavelength, a test of previously developed parametrizations [3, 6] is possible. Within this paper, we will focus on the empirical analysis of the reflectivity data and the microscopic reasoning for a finite width of the shock front.

2. Finite shock front width

We assume a planar shock front propagating in the z direction (normal incidence). A density profile $n(z)$ of the shock wave front is considered, assuming the free electron density increases smoothly from zero in front of the shock front to its maximum value n_e behind the shock front, see [1, 2, 4]. If this maximum value n_e is above $n_e^{cr}(\lambda)$, the reflection of electromagnetic radiation occurred already in the outer region where the density is low. Within a simplified picture, the radiation penetrates the low-density region of the plasma up to the region where the density approaches the critical value. Here the wave is reflected.

More rigorously, the reflectivity R from a given charge density profile can be obtained from the direct solution of the Maxwell equations. Neglecting non-local effects for the conductivity, we consider the Helmholtz equation [12] for the complex amplitude of the electric field $E(\omega_L, z)$,

$$\frac{d^2E(\omega_L, z)}{dz^2} + \frac{\omega_L^2}{c^2}\epsilon(\omega_L, z)E(\omega_L, z) = 0. \tag{2}$$

The dielectric function $\epsilon(\omega_L, z)$ is calculated from (1) for given density and temperature profiles $n(z)$, $T(z)$. Different approaches for the collision frequency accounting for frequency dependence, contribution of neutral bound states, etc have been considered in previous publications of the authors [3, 6, 8]. In this context, it has been shown that the following approximations are sufficient. We use the interpolation formula for the static conductivity as derived by Esser *et al* [13] in the approximation $\nu_{dc}(n, T) = (ne^2/m_e)\,\sigma_{dc}^{-1}(n, T)$. Then

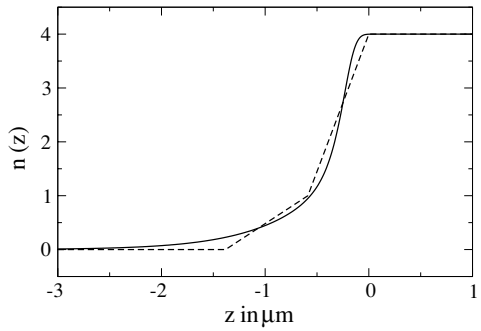

Figure 1. Comparison between the bi-linear profile (dashed line) [3] and asymmetric Fermi profile (3) (solid line) fitted to the reflectivity R at $n_e = 4 \times 10^{21}$ cm^{-3}.

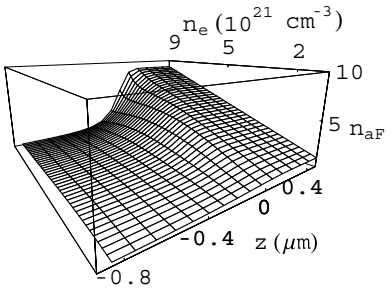

Figure 2. Profile of the shock front density $n_{aF}(n_e, z)$, equation (3) for different maximum densities n_e.

equation (2) is solved numerically starting from the initial point z_0. The reflectivity is given by $R = |E_r(z_1)|^2/|E_i(z_1)|^2$, where $E_i(z)$ and $E_r(z)$ describe incident and reflected waves, respectively, at the free space region z_1 ($\epsilon(\omega, z_1) = 1$).

For now, we consider a density profile as a given quantity; for a microscopic approach see below. The temperature is assumed to be uniform at the plasma temperature throughout the shock wave front. Smooth empirical density profiles for a shock wave front such as a linear decrease or a spatial variation according to a Fermi function have been considered in various combinations [3, 6, 8, 14]. As already mentioned in [1], the density profile across the shock front is expected to increase at first slowly and become steeper towards the plasma region. Such a behaviour was already reproduced using a bi-linear profile [3]. The disadvantage of this previously-assumed continuous profile consisting of two Fermi functions [3] was its symmetry with respect to the gradual changes at the boundary of the profile. Therefore, we now propose an asymmetric Fermi profile:

$$n_{aF}(n_e, z) = \frac{n_e}{e^{Y(z)} + 1}, \tag{3}$$

$$Y(z) = -\frac{z}{A} - e^{z/B} + C. \tag{4}$$

For an appropriate parameter set, this profile is shown in figure 1 in comparison to the bi-linear profile. As shown in figure 2, the expected general behaviour of the density profile is reproduced. For the suitably chosen parameters A, B, C see the following section. In particular, the parameter A affects the width of the ordinary Fermi profile in the low density

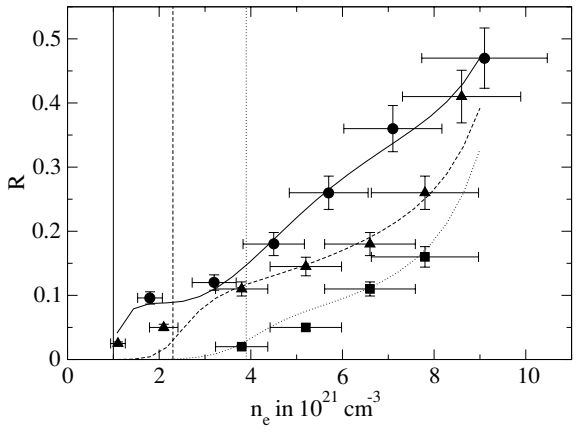

Figure 3. Reflectivity coefficient R for xenon calculated with asymmetric Fermi profile n_{aF} (lines) in comparison with measurements (symbols with error bars) [1, 2, 4] for laser wavelengths 1.06 μm (solid line, ●), 0.694 μm (dashed line, ▲) and 0.532 μm (dotted line, ■), the corresponding critical densities $n_{\mathrm{e}}^{\mathrm{cr}}$ are indicted with vertical lines.

region for negative z. The second parameter B influences the order of asymmetric compression in the high-density region for positive z. With the last parameter C one is able to choose the point where the ordinary Fermi function starts to be compressed. The details of the density profile can be controlled by measuring the reflectivity at different laser frequencies ω_{L}. As will be shown in the next section, we are able to justify the ansatz equation (3) in an empirical way. In detail, we use two different laser frequencies ω_{L} to determine the parameters of the density profile equation (3) and show that the experimental values of the reflectivity R for a third laser frequency are also well reproduced.

3. Parametrization of the density profile

Using measurements of the reflectivity at different wavelengths, it is possible to determine the details of the density profile. We use the ansatz equation (3) with open parameters A, B, C. The parameters were fitted to reproduce the experimental values for the wavelengths 1.06 μm and 0.694 μm. Interpolating for the reflectivity between different density values n_{e} in the plasma according to the experiments [1, 2, 4], we found the following parametrization for the profile:

$$\begin{aligned} A(n_{\mathrm{e}}) &= a_1 + a_2 \cdot \mathrm{e}^{a_3 \cdot n_{\mathrm{e}}}, \\ B(n_{\mathrm{e}}) &= b_1 \cdot n_{\mathrm{e}}^3 + b_2 \cdot n_{\mathrm{e}}^2 + b_3 \cdot n_{\mathrm{e}} + b_4, \\ C(n_{\mathrm{e}}) &= c_1 \cdot n_{\mathrm{e}}^2 + c_2 \cdot n_{\mathrm{e}} + c_3 \end{aligned} \tag{5}$$

and $a_1 = 0.032\,54$ $a_2 = 1.437$, $a_3 = -0.4909$, $b_1 = -0.003\,687$, $b_2 = 0.057\,75$, $b_3 = -0.2560$, $b_4 = 0.479\,05$, $c_1 = 0.031\,55$, $c_2 = -0.055\,37$, $c_3 = 0.4720$. The densities have to be taken in units of 10^{21} cm^{-3} and the position z in μm. A landscape of the density profiles for different values of n_{e} is shown in figure 2.

The results for the reflectivity R, calculated for the asymmetric Fermi profile $n(n_{\mathrm{e}}, z)$, equation (3) and fixed temperature $T = 33\,000$ K are shown in figure 3 for three different laser frequencies ω_{L}. The critical densities are indicated. Above those, the reflectivity R starts to increase. Also experimental values are shown. As in former works [3, 6, 8, 14], the

experimental values at laser wavelengths 1.06 μm and 0.694 μm are well reproduced. Data at the third wavelength of 0.532 μm have then been calculated from the derived shock wave profiles. The experimental data are reproduced within the error bars except in the region of very low densities. The surprisingly good qualitative agreement shows that the adjustment of the parameters using two wavelengths is sufficient to describe the behaviour of the reflectivity for the third wavelength and probably other wavelengths as well.

4. Transport and radiation effects in the shock wave front

As shown in the previous sections, the experimental values for the reflectivities are well explained using a smooth density profile, so that the shock wave front is smeared out over a range of 0.1–1.0 μm. However, a microscopic approach is needed to give a justification of this empirical ansatz. We discuss some effects which lead to a softened profile instead of a step-like density profile.

A first discussion can be given with respect to local equilibrium and charge neutrality. At typical parameter values $n_e \approx 10^{21}$ cm^{-3} and $T = 33\,000$ K, the mean free path of the electrons $l_e = \sqrt{k_B T/m_e}\nu_{dc}^{-1}$ results in 1.55 nm so that the scale is far below the μm scale. Similarly, the Debye length $\lambda_D = \sqrt{\epsilon_0 k_B T/(e^2 n_e)}$ is 1.4 nm, so that the distance at which free electrons spread out into the low-density region in front of the shock front is also very small in comparison to the μm scale, see also [15]. Thus, neither effect is appropriate to explain the empirically obtained density profile.

Assuming local equilibrium, a hydrodynamic description of the density and temperature profile is possible. Hydrodynamic investigations with the program package MULTI [16] were performed. Using a real gas equation of state without transport processes and simulating the propagation of a high speed target into the homogenous material, a step-like profile results. Traditionally [17], the description of the shock wave front is done using the hydrodynamic equations leading to the Hugoniot equation for a sharp shock wave front. The experimentally observed shock wave velocities can be reproduced very well. However, we should also take into account dissipative effects. The inclusion of viscosity in the momentum and energy balance equations and the thermal conductivity κ in the energy balance can be done [18] and leads to a nonlinear differential equation of second order for the position-dependent velocity. Some further approximations, which are justified in our parameter range as checked by comparing with the numerical solution, allow an estimate for the width of the shock wave [18]

$$\Delta z = \frac{2(\gamma - 1)}{\gamma + 1} \frac{\kappa m_{Xe}}{\rho(v_p - v_s)k_B} \left(\frac{2v_p}{v_s} - 1\right) \ln\left(\frac{1}{\delta} - 1\right), \tag{6}$$

where v_p and v_s are the velocities of the piston and the shock wave, respectively. ρ is the mass density in the plasma and δ is the relative deviation of the velocity from the velocity at infinity. For the mono-atomic ideal gas, we have $\gamma = 5/3$. Hirschfelder *et al* [18] give a thermal conductivity κ of 5.5×10^{-3} W (K m)$^{-1}$ for neutral xenon gas if considered as a Lennard-Jones system. Thus the shock wave width is determined within a hydrodynamic approach to be about 1–2 nm, several orders of magnitude narrower than we had to assume in order to fit the experimental data. We conclude that the assumption of local equilibrium for the hydrodynamic description is not able to produce a smooth density profile.

Ionization caused by thermal radiation from the heated plasma could lead to more free charge carriers in front of the shock wave. We have calculated the maximum possible free electron density using the program package COMPTRA04 [19]. It determines the thermodynamic properties under the assumption of coupled mass action laws for atoms and

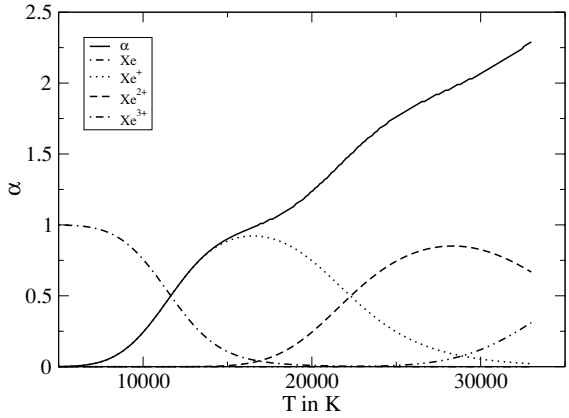

Figure 4. Degree of ionization α (solid line) over temperature computed by COMPTRA04 [19] at $n = 1.24 \times 10^{20}$ cm^{-3}. The relative proportions of relevant ions are also represented.

ions taking into account non-ideality corrections in the virial expansions. The total density was assumed to be the initial density before the compression of xenon. The temperature was then varied up to a maximum of about 33 000 K. An example is shown in figure 4 where the initial total density was taken as 1.24×10^{20} cm^{-3}. We find that the maximum free electron density is reached at the maximum temperature, as expected. Since the initial densities are so low, even the observed ionization degree of $\alpha = 2.4$ leads only to a free electron density of 3×10^{20} cm^{-3}, which is below the critical densities n_e^{cr}, see table 1. A precursor of free electron density due to radiative heating is not sufficient to explain the absolute smooth density profile.

5. Conclusion

The reflectivity on shock-compressed plasma has been calculated and compared with experimental results on Xe which have been observed for three different wavelengths. The empirical assumption of a spatially extended finite shock wave front leads to a good agreement with the experimental data. However, the discussion on possible scenarios which cause this shock wave front is still unsatisfying. Within hydrodynamic considerations and simulations, microscopic processes which lead to a finite shock wave front are discussed. Under the assumption of local equilibrium, neither dissipative processes in the hydrodynamic equations nor radiation transport seem to give the expected width of the front. The validity of this assumption and the use of kinetic equations should be investigated. So far, we have assumed a plane shock wave surface. Here, work is in progress.

Acknowledgments

The authors HR, GR and TR express their thanks for the great hospitality during the SCCS conference in Moscow as well as the financial support by INTAS Conference Organization Grant, INTAS Ref no 05-98-001. Furthermore, we acknowledge fruitful discussions with V Gryaznov, A Kemp, M Marti, J Meyer-ter-Vehn, I Morozov and A Tronnier. The work has been supported by the Graduiertenkolleg 567 'Strongly-coupled many-body systems' and the Sonderforschungsbereich SFB 652 'Strong correlations and collective phenomena in radiation fields: Coulomb systems, clusters and particles'.

References

[1] Mintsev V and Zaporoghets Y 1989 *Contrib. Plasma Phys.* **29** 493
[2] Zaporoghets Yu B, Mintsev V B, Gryaznov V K and Fortov V E 2002 *Physics of Extreme States of Matter* ed V E Fortov *et al* (Chernogolovka) p 188 (in Russian)
[3] Reinholz H, Röpke G, Morozov I, Mintsev V, Zaparoghets Y, Fortov F and Wierling A 2003 *J. Phys. A: Math. Gen.* **36** 5991
[4] Zaporoghets Y, Mintsev V, Gryaznov V, Fortov V, Reinholz H, Raitza T and Röpke G 2006 *J. Phys. A: Math. Gen.* **39** 4329
[5] Rozmus W, Tikhonchuk V and Cauble R 1996 *Phys. Plasmas* **327** 360
[6] Reinholz H, Röpke G, Wierling A, Mintsev V and Gryaznov V 2003 *Contrib. Plasma Phys.* **43** 3
[7] Reinholz H, Redmer R, Röpke G and Wierling A 2000 *Phys. Rev.* E **62** 5648
[8] Reinholz H, Zaparoghets Y, Mintsev V, Fortov V, Morozov V and Röpke G 2003 *Phys. Rev.* E **68** 036403
[9] Kurilenkov Y, Berkovsy M, Hocini S and Skowronek M 1995 *J. Phys. B: At. Mol. Opt. Phys.* **28** 2021
[10] Berkovsky M, Kurilenkov Y and Milchberg H 1992 *Phys. Fluids* B **4** 2423
[11] Desjarlais M P 2005 *Contrib. Plasma Phys.* **45** 300
[12] Lekner J 1987 *Theory of Reflection* (Dordrecht: Martinus Nijhoff)
[13] Esser A, Redmer R and Röpke G 2003 *Contrib. Plasma Phys.* **43** 33
[14] Raitza T 2005 *Master's Thesis* Universität Rostock
[15] Mora P 2003 *Phys. Rev. Lett.* **90** 185002
[16] Ramis R, Schmalz R and Meyer-ter-Vehn J 1998 *MULTI—A Computer Code for One-Dimensional Multigroup Radiation Hydrodynamics* (Garchingen: MPI Quantenoptik)
[17] Zeldovich Z B and Raizer Y P 1966 *Physics of Shock Waves and High-Temperature Hydrodynamic Phenomena* vol 1 ed W D Hayes and R F Probstein (New York: Academic)
[18] Hirschfelder J O, Curtiss C F and Bird R B 1954 *Molecular Theory of Gases and Liquids* (New York: Wiley)
[19] Kuhlbrodt S, Holst B and Redmer R 2005 *Contrib. Plasma Phys.* **45** 73